

Perceptron Synthesis Network: Rethinking the Action Scale Variances in Videos

Yuan Tian¹, Guangtao Zhai¹, Zhiyong Gao¹

¹Institute of Image Commu. and Network Engin., Shanghai Jiao Tong University, China

Abstract

Video action recognition has been partially addressed by the CNNs stacking of fixed-size 3D kernels. However, these methods may under-perform for only capturing rigid spatial-temporal patterns in single-scale spaces, while neglecting the scale variances across different action primitives. To overcome this limitation, we propose to learn the optimal-scale kernels from the data. More specifically, an *action perceptron synthesizer* is proposed to generate the kernels from a bag of fixed-size kernels that are interacted by dense routing paths. To guarantee the interaction richness and the information capacity of the paths, we design the novel *optimized feature fusion layer*. This layer establishes a principled universal paradigm that suffices to cover most of current feature fusion techniques (e.g., channel shuffling and channel dropout) for the first time. By inserting the *synthesizer*, our method can easily adapt the traditional 2D CNNs to the video understanding tasks such as action recognition with marginal additional computation cost. The proposed method is thoroughly evaluated over several challenging datasets (i.e., Something-to-Something, Kinetics and Diving48) that highly require temporal reasoning or appearance discriminating, achieving new state-of-the-art results. Particularly, our low-resolution model outperforms the recent strong baseline methods, i.e., TSM and GST, with less than 30% of their computation cost.

Introduction

Video action recognition has draw much attentions in computer vision community for its tremendous applications (Tian et al. 2019). Inspired by the breakthrough brought by CNNs on still image recognition task, recent video recognition methods also leverage the 2D CNNs expanded with temporal modeling ability, particularly the 3D CNNs, for spatial-temporal modeling.

3D convolutions are the main operation in the 3D CNNs, which learn spatial-temporal filters to capture visual cues and dynamics of the objects simultaneously. To constrain the parameter number and the computation cost of the whole architecture, most 3D CNNs tend to utilize the filters of typical size $3 \times 3 \times 3$, resulting in a relatively small receptive field. Stacking the small filters and downsampling the features after each stage can enlarge the receptive field to cover the whole input clip. However, there are two issues that limit the performance of down stream tasks. (a) The *scale* of receptive field *w.r.t.* each layer is fixed, thus the actions of big

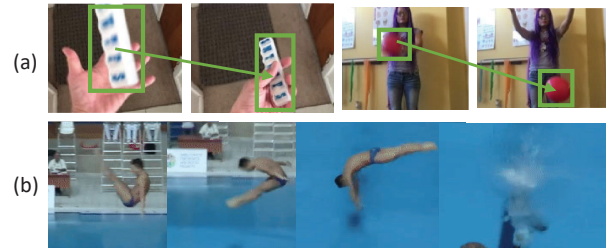


Figure 1: (a) Examples from the Something-Something dataset (Goyal et al. 2017). The motion degree (i.e., the green arrow line) and the scale of moving object (i.e., the area of green square box) of different samples are drastically distinct from each other. (b) Example video of “forward and PIKE” from the Diving48 (Li, Li, and Vasconcelos 2018). The action can only be recognized by first discriminating the short-term action primitives and then reasoning the long-term dependence order. Therefore, a powerful method that suffices to handle diverse action variances (in both of spatial and temporal spaces) is critical.

objects can only be detected in the deeper layers, resulting in the loss of fine-grained details. (b) The spatial-temporal *aspect ratio* of receptive field is also fixed, which relies on the hand-crafted tuning for datasets of different complexities.

Particularly, the spatial-temporal scale variation is an essential property of the natural actions in the wild. As shown in Fig. 1, in single frame, some objects occupy a rather large spatial spaces (e.g., humans) while some other objects (e.g., socket and ball) only take up a relatively smaller spatial region. The issue becomes more serious when considering the object variance along the temporal axis: the same object may show different scales across different frames for the deformation of itself or the changing of the camera viewpoint. Moreover, tolerating the actions of different complexity is also another challenge. For the simple actions composed of one or two stages, such as that from the Something-Something dataset (Goyal et al. 2017), the actions can be classified accurately by simply observing the short-term state changes within 2 or 3 frames. Conversely, the complex actions in Diving48 (Li, Li, and Vasconcelos 2018) require the long-term comprehensive understanding of the phased changes. To capture such a diversity of object spatial scales and action durations, utilizing a *single* and

fixed type of kernel with a rigid spatial-temporal receptive field can not handle complex scale variances and thus results in performance degradation. For image recognition, one of the most popular architecture for multi-scale modeling is the Inception networks (Szegedy et al. 2016). However, simply extending this architecture to its 3D version maybe sub-optimal because the extended spatial-temporal cube-shaped kernels, *e.g.*, $3 \times 3 \times 3$ and $5 \times 5 \times 5$, are not able to reach the best performance, as shown in the ablation studies.

So, how to decide the optimal-size kernels? Our answer is to learn it from the data. Instead of simply utilizing the NAS (neural architecture search) (Zoph and Le 2016) as in (Piergiovanni, Angelova, and Ryoo 2019), which involves training hundreds of models with huge computation cost, we seek for a soft fusion of the candidate fixed-size kernels with only *one-time* training. More specifically, we propose an *action perceptron synthesizer* to continuously generate rich-scale filters from the candidates under the optimization goal: towards the best accuracy for action classification. When the process finished, we freeze the synthesizer and utilize the produced filter group as the optimal. To fully exploit the inter-relations between the fixed-size filters and retain the network capacity to the utmost extent, we propose a novel *optimized feature fusion layer* as a component of the synthesizer, which provides the dense learnable routing paths among the filters. This layer covers most feature fusion techniques as special cases of it, *e.g.*, channel shuffling (Zhang et al. 2018) and channel dropout. In the experiment part, we demonstrate that the proposed layer achieves conspicuous performance improvement while only introducing marginal learnable parameters and computation cost compared with other conventional feature fusion methods.

Unlike the previous works utilizing single-scale kernels, the synthesizer allows us to deeply exploit the adaptive interactions within the multi-scale spatial and temporal information in each layer when trained on different datasets. By analyzing the statistical distribution of the produced kernels, we demonstrate a series of *interpretable insights* in the experiment part, which are useful for the hand-crafted designing of future video networks.

We summarize our contributions as follows:

- To cope with the essential spatial-temporal scale variances in the videos, we propose a novel *action perceptron synthesizer* to generate the optimal-size kernels in each layer instead of simply leveraging the ordinal single-scale kernels of fixed-size.
- We propose an *optimized feature fusion layer* as a component of the synthesizer to facilitate the inter-connections between the features from different branches, which outperforms other feature fusion methods conspicuously with negligible parameters and costs.
- We perform an extensive ablation analysis of the proposed method and also show some network designing insights from the searching process of the optimal kernel.
- We achieve state-of-the-art on several large scale video datasets with comparable parameters and FLOPs compared to existing approaches.

Related Works

Deep Video Recognition

Simonyan *et al.* (Simonyan and Zisserman 2014a) first proposed the Two-stream framework. Feichtenhofer *et al.* (Feichtenhofer, Pinz, and Zisserman 2016) then improved it. Later, TSN (Wang et al. 2018a) proposes a new sparse frame sampling strategy. 3D networks, *e.g.*, C3D network (Tran et al. 2015), I3D (Carreira and Zisserman 2017), 3D-ResNet (Hara, Kataoka, and Satoh 2017; Tian et al. 2020), R(2+1)D CNNs (Tran et al. 2018)(Qiu, Yao, and Mei 2017) and Slowfast networks (Feichtenhofer et al. 2019), recently have gained much attention as another research line.

Multi-scale CNN Architectures

CNNs are naturally equipped with multi scale feature representation ability due to the hierarchical stacking of convolution kernels, *e.g.*, VGGNet (Simonyan and Zisserman 2014b) and ResNet (He et al. 2016). Modern CNN architectures design the multi-scale branches explicitly. The GoogLeNet (Szegedy et al. 2015) utilizes diverse filters with different kernel sizes in parallel to encode the multi-scale feature in each branch. Latter, the Inception Nets (Szegedy et al. 2016)(Szegedy et al. 2017) propose to utilize more small filters in each branch of the parallel branches in the GoogLeNet (Szegedy et al. 2015) to further expand the receptive field.

Efficient Neural Network Designing

Grouped convolution is first introduced in AlexNet (Krizhevsky, Sutskever, and Hinton 2012) and then widely used in later networks, *e.g.*, ResNeXt (Xie et al. 2017), for efficient computing. Depthwise convolution is the special case of grouped convolutions, where the feature channel of each group is single. Recent compact models running on mobile platforms such as MobileNetV2 (Sandler et al. 2018) and ShuffleNet (Zhang et al. 2018)(Ma et al. 2018) leverage the depthwise convolution extensively and achieve effective results. Particularly, ShuffleNet (Zhang et al. 2018) proposes a novel channel shuffling operation for fusing the features produced by different group of convolution filters.

Approach

In this section, we first propose that the optimal-size spatial-temporal kernel for video modeling can be decomposed into multi-scale spatial and temporal kernels of fixed-size fused by a learnable weight matrix. We further demonstrate that the weight matrix shall obey some explicit constraints and propose an optimized feature fusion layer. Finally, we instantiate our method as an action perceptron synthesizer block and develop a new video modeling network upon the block with an efficient architecture and high performance.

Optimal Spatial-temporal Kernel Approximation

We first postulate there exists an *ideal* video CNN, where each layer transforms a 4-dimensional input tensor U of size $C \times T \times W \times H$ into an output tensor V of the same size,

$V = U * \hat{F}$, where \hat{F} is the *optimal* convolution kernel with the receptive field of size $\hat{T} \times \hat{W} \times \hat{H}$. The optimization goal of our method is to approximate \hat{F} precisely under the assumption that the upper bound of its receptive field is $L \times L \times L$.

We propose to synthesize the *unknown* \hat{F} by approximating the produced V as :

$$\tilde{V} = \sum_{i=1}^G W'(i) \odot \left(\sum_{j=1}^G W(j) \odot U * F_s^{(2j-1) \times (2j-1) \times 1} \right) * F_t^{1 \times 1 \times (2i-1)}, \quad (1)$$

where G denotes the number of branches of different kernel, \odot denotes the channel-wise multiplication. Each element of W' and W is a C -length vector, indicating the channel-wise importance of the tensor produced by the kernels. We show the derivation process in the *supplementary material*. Although the representation seems to share some similarities with the R(2+1)D CNNs (Tran et al. 2018), the focus of our method is to produce filters of *diverse scales and shapes* instead of only saving the computation cost.

The physical meaning behind the Eq. (1) is that the optimal-size spatial-temporal kernel \hat{F} can be *mimicked* by a bag of multi-scale spatial kernels $F_s = \{F_s^{1 \times 1 \times 1}, \dots, F_s^{L \times L \times 1}\}$ followed by another bag of multi-scale temporal kernels $F_t = \{F_t^{1 \times 1 \times 1}, \dots, F_t^{1 \times 1 \times L}\}$. The two bags are interacted by W (W' is only related to the temporal kernels).

In the next section, we discuss the constraints of W under the group convolution setting, *i.e.*, (1) $U = U_1 \oplus U_2 \oplus \dots \oplus U_G$, where G denotes the group number. (2) Each kernel of F_s and F_t only performs on the one group.

Optimized Feature Fusion Layer

Given the feature $X = X_1 \oplus X_2 \oplus \dots \oplus X_G$ produced by spatial convolutions in Eq. (1), $X_j = U_j * F_s^{(2j-1) \times (2j-1) \times 1}$, where $j \in [1, G]$. Now, we assume there exists a block transformation matrix $\mathcal{T} \in \mathbb{R}^{G \times G}$ performing on X to produce $Y = Y_1 \oplus Y_2 \oplus \dots \oplus Y_G$, as shown in Fig. 2. Noting that \mathcal{T} of size $G \times G$ is reshaped from W in Eq. (1) of size G by dividing the each element of it into G groups. Each element of \mathcal{T} is a c -element vector, which is consistent with the channel number of X_j and Y_i , where $c = \frac{C}{G}$. We formulate the transformation process above as: $Y = \mathcal{T} \times X$, where the multiplication between each element of \mathcal{T} and X is channel-wise. In the following parts, we omit the domain of $i, j \in [1, G]$.

We quantify the routing paths between the spatial and temporal kernels of different size by: *ir - interactions* = $\sum_{i=1}^G \sum_{j=1}^G N_{X_i \rightarrow Y_j}, i \neq j$, where $N_{X_i \rightarrow Y_j}$ denotes the information flowed from X_i to Y_j , which is measured by the number of feature channels. *ir - interactions* indicates the number of the synthesized *irregular-shaped* spatial-temporal kernels, compared to the regular-shaped kernels of size $3 \times 3 \times 3$ or $5 \times 5 \times 5$. In the experiment part, we show that this metric has strong impact on the performance.

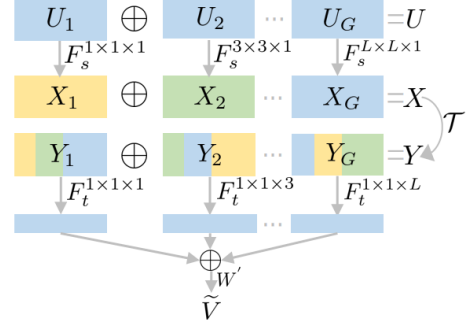


Figure 2: Schematic representation of Eq. (1) under the group convolution setting. The core of the *optimized feature fusion layer* is a constrained transformation matrix \mathcal{T} , which is *reshaped* from the W in Eq. (1). \oplus denotes the channel concatenation operation.

Optimization goal: (1) Spatial-temporal interaction richness. We propose the interaction loss formulated as:

$$\mathcal{L}_{interaction} = -\frac{1}{G^2} \sum_{i=1}^G \sum_{j=1}^G \text{sigmoid}(\|\mathcal{T}_{ij}\|_1), \quad (2)$$

where $\|\cdot\|_1$ denotes the ℓ_1 norm. This loss facilitates higher inter-group interaction richness of X while regularizing the weights not exploding. By this way, the temporal convolutions after the fusion layer can receive very rich-scale spatial features. In practice, we find the *ir - interactions* tends to be $G^2 \cdot c$ when utilizing this loss.

(2) High network capacity. We propose the network capacity loss formulated as:

$$\mathcal{L}_{capacity} = \frac{1}{G^2} \sum_{i=1}^G \sum_{j=1}^G \frac{\text{avg}(Y_i) \cdot \text{avg}(Y_j)}{\|\text{avg}(Y_i)\|_2 \|\text{avg}(Y_j)\|_2}, \quad (3)$$

where avg denotes the spatial-temporal average pooling operation, \cdot and $\|\cdot\|_2$ denotes Dot product and ℓ_2 norm respectively. This loss facilitates the lower inter-group similarity within Y and thus leads to the wider network of higher capacity in essence.

vs. Other feature fusion techniques. We assume that each weight vector \mathcal{T}_{ij} in \mathcal{T} is also sub-grouped into G groups: $\mathcal{T}_{ij} = \mathcal{T}_{ij}(1) \oplus \dots \oplus \mathcal{T}_{ij}(G)$. Then, under the framework of the proposed layer, channel shuffling (Zhang et al. 2018) can be represented as:

$$\begin{cases} \mathcal{T}_{ij}(k) = \mathbf{1}, k = i, \\ \mathcal{T}_{ij}(k) = \mathbf{0}, \text{others.} \end{cases}, \quad (4)$$

where $k \in [1, G]$, $\mathbf{1}$ and $\mathbf{0}$ denote *all-one* and *all-zero* vectors of size $\frac{c}{G}$ separately. Further comparing with other conventional feature fusion techniques as a special cases of our method is in the *supplementary material*.

Action Perceptron Synthesizer

We wrap the approximated optimal spatial-temporal operation in Eq. (1) into an action perceptron synthesizer that can be incorporated into many existing architectures. The

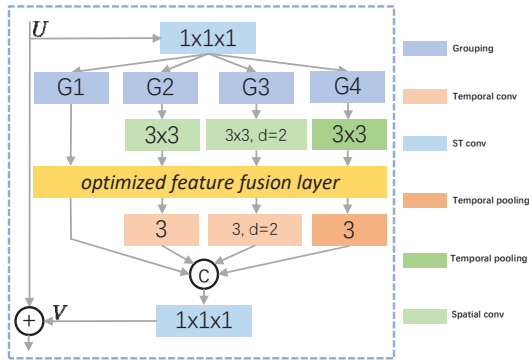


Figure 3: An example Action Perceptron Synthesizer of maximum receptive field $5 \times 5 \times 5$. \odot and \oplus denotes the channel-wise concatenation and element-wise summation operation respectively. All the filters are performed on the grouped features for efficient computation. The blocks marked with “d” are dilated convolutions. The *optimized feature fusion layer* can be implemented as a fully-connected layer regularized by $\mathcal{L}_{interaction}$ and $\mathcal{L}_{capacity}$.

synthesizer is defined as: $z_i = V_i + U_i$, where V_i is given in Eq. (1) and “ $+U_i$ ” denotes a residual connection (He et al. 2016). The residual connection allows us to insert the proposed synthesizer into any pre-trained model such as ResNet, without breaking its initial behavior (e.g., when W in Eq. (1) is initialized as zero). An example action perceptron synthesizer is illustrated in Fig. 3. The *optimized feature fusion layer* can be simply implemented as a fully connected layer while regularized by the two proposed losses. Only spatial convolutions are followed by the batch normalization (BN) (Ioffe and Szegedy 2015) and ReLU non-linearity (Nair and Hinton 2010). We also add the max-pooling branch, which improves the performance obviously due to its complement for convolution operations.

Video Perceptron Synthesis Networks. The proposed action perceptron synthesizer is flexible and can be easily integrated with most of the current 2D or 3D CNNs. More specifically, we adopt 2D-ResNet-50 (He et al. 2016) as the backbone networks and insert the proposed synthesizer between the residual blocks. The final prediction is a simple average pooling of the results from each frame. We conduct extensive experiments on the different variants of it.

End-to-end learning for action recognition. Finally, we apply the proposed networks to the action recognition task. The total loss is given by $\mathcal{L} = \mathcal{L}_{classification} + \alpha\mathcal{L}_{interaction} + \beta\mathcal{L}_{capacity}$, where $\mathcal{L}_{classification}$ is the cross-entropy loss, α and β are the balancing weights.

Experiments

Video Datasets

Something-Something. This dataset includes v1 (Goyal et al. 2017) and v2 (Mahdisoltani et al. 2018). We mainly conduct ablation experiments and justify each component on Something-Something v1 dataset.

Kinetics. Kinetics (Carreira and Zisserman 2017) is a challenging human action recognition dataset. The actions in this

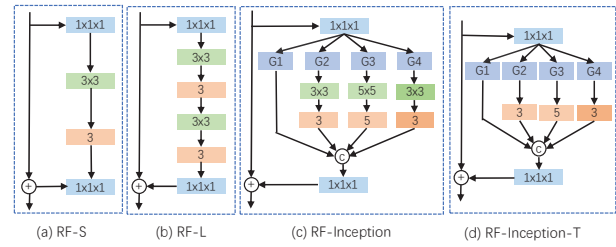


Figure 4: Illustrations of the baseline methods. The representation signs are the same meaning with Fig. 3. “RF” is abbreviated from “receptive field”. The convolutions of kernel size 5 are also implemented as their dilated counterparts.

dataset mainly rely on the appearance of the objects and the background scenes to be discriminated.

Diving48. Diving48 (Li, Li, and Vasconcelos 2018) is a new dataset with more than 18K video clips for 48 unambiguous diving classes, requiring multi-scale temporal modeling. We report the accuracy on the official train/val split.

Implementation Detail

We implement our model in Pytorch (Paszke et al. 2019). We adopt ResNet50 (He et al. 2016) pretrained on ImageNet (Deng et al. 2009) as the backbone. The parameters within the action perceptron synthesizers are randomly initialized. The synthesizers are inserted after the $conv_{1-4}$ if no specified otherwise. For the temporal dimension of the input clips, we use the sparse sampling method described in TSN (Wang et al. 2016). For spatial dimension, the short-side of the input frames are resized to 256 and then cropped to 224×224 . We do random cropping and flipping as data augmentation during the training. We train the network with a batch-size of 64 on 8 NVIDIA GTX-2080Ti GPUs and optimize it using SGD with an initial learning rate of 0.01 for 50 epochs and decay it by a factor of 10 every 10 epochs. The total training epochs are about 80. To train the total loss, we set the balancing weights of the losses as: $\alpha = 0.01$ and $\beta = 0.001$ by grid searching. The dropout ratio is set to be 0.3 as in (Luo and Yuille 2019). During the inference, we sample the middle frame in each segment and do center crop for each frame. We report the results of **1 crop** unless specified. Note that many state-of-the-art methods report their final performances with 5 or 10 crops, which enlarge the inference-time computation cost by 5 or 10 times. Moreover, we only use **RGB modality** as the input to our model.

Ablation Study

We conduct extensive ablation studies on the Something-Something V1 (Goyal et al. 2017) dataset to demonstrate the effectiveness of every aspects of our method. All the synthesizers in these experiments are of maximum receptive field $5 \times 5 \times 5$ as shown in Fig. 3 and performed on the $1/4$ proportion of input features if no specified otherwise. To facilitate the training process, in these experiments, we adopt a smaller input resolution: the short-side of the input frames are resized to 128 and then the frames are cropped to 112×112 .

Methods	Backbone	Maximum RFS	Synthesized kernel shapes	Irregular shape?	Multi-scale?	Parameters	Sth v l	
							Top1 (%)	Top5 (%)
TSN (Wang et al. 2016) [†]	ResNet50	-	-	-	-	23.87M	14.90	36.97
TSM (Lin, Gan, and Han 2019) [†]	ResNet50	1 × 3	1	✓	-	23.87M	42.11	71.01
GST (Luo and Yuille 2019) [†]	ResNet50	3 × 3	1	-	-	21.04M	42.36	71.42
GST (Luo and Yuille 2019) [†]	ResNet101	3 × 3	1	-	-	37.52M	41.16	69.76
RF-S	ResNet50	3 × 3	1	-	-	27.57M	43.72	73.14
RF-L	ResNet50	5 × 5	1	-	-	27.35M	43.67	71.88
RF-L-Inception	ResNet50	5 × 5	4	-	✓	27.56M	43.84	72.59
RF-L-Inception-T	ResNet50	1 × 5	4	✓	✓	27.28M	44.23	72.87
Ours	ResNet50	5 × 5	16	✓	✓	27.55M	45.44	74.12
Ours-1/16	ResNet50	5 × 5	16	✓	✓	24.05M	44.00	72.65

Table 1: Results of inserting different spatial-temporal blocks to 2D ResNet-50. The evolution of the performance improvement can be explained by diverse shape synthesized kernels, especially the introduction of irregular shape kernels, and multi-scale designing. [†] indicates that the results are reproduced under the same input size with us.

Methods	$ir - interactions$	Dropout rate	Parameters	Sth v l	
				Top1 (%)	Top5 (%)
Channel grouping	0	0	0M	43.84	72.59
Channel dropout	1856	0.75	0M	44.64	73.03
Channel shuffling	1856	0	0M	45.01	73.53
Ours	< 1856	> 0	0.086 M	45.44	74.12
Ours+ \mathcal{L}_i	~ 1856	> 0	0.086 M	46.12	74.92
Ours+ \mathcal{L}_c	< 1856	0	0.086 M	45.88	74.22
Ours+ \mathcal{L}_i and \mathcal{L}_c	~ 1856	0	0.086 M	46.41	75.01

Table 2: Comparison of different feature fusion methods. Larger $ir - interactions$ and lower dropout rate bring more performance gain. \mathcal{L}_i and \mathcal{L}_c denotes $\mathcal{L}^{interaction}$ and $\mathcal{L}^{capacity}$ respectively. Architecture details are in *supplementary material*.

Design	Parameter number	Sth v l	
		Top1 (%)	Top5 (%)
Avg Pool	27.55M	45.42	73.98
Max Pool	27.55M	45.44	74.12
Without Max Pool	27.55M	44.19	73.45
Max Pool	27.55M	45.44	74.12
Without inter ReLU	27.55M	44.65	73.30
Inter ReLU	27.55M	45.44	74.12
Without dilation	27.95M	45.54	73.09
Dilation	27.55M	45.44	74.12
(1+1)D	27.45M	45.17	73.77
(2+1)D	27.55M	45.44	74.12

Table 3: Detailed design of the proposed block.

To emphasize the importance of two important philosophies in our method: (a) *multi-scale modeling* and (b) *optimal-size kernels synthesizing* especially the *irregular-shaped* kernels, we compare against the following baselines: (1) The vanilla TSN (Wang et al. 2016), (2) **RF-S model** shown in Fig. 4 (a), (3) **RF-L model** shown in Fig. 4 (b), (4) **RF-L-Inception model** shown in Fig. 4 (c), (5) **RF-L-Inception-T model** shown in Fig. 4 (d). The architecture details are in the *supplementary material*.

The superiority of action perceptron synthesizer As shown in Tab. 1, our method mine the spatial-temporal reasoning information much better. Compared with the RF-L-Inception model, our method improves the performance significantly with almost no extra computation cost, thanks to the kernels of much more diverse shapes (16 vs. 4), especially the irregular shape, introduced by the *synthesizers*.

Also, *multi-scale* modeling widely adopted in the modern CNNs only contributes marginal performance gain: *0.17%* (RF-L vs. RF-L-Inception) whereas *rich kernel shape* brings conspicuous improvement: **1.60%** (RF-L-Inception vs. our method) in terms of Top1 accuracy. Interestingly, only enlarging the maximum receptive field in a naive way, *i.e.*, from RF-S model to RF-L model, the performances are degraded slightly. We conjecture that the degradation is caused by the smaller enhanced spatial-temporal *feature proportion* of RF-L model (1/6 vs. 1/8), which will be discussed in *supplementary material*. The large performance improvement of RF-L-Inception-T upon TSM also proves the merits of *learnable multi-scale* temporal modeling. To compare with TSN and TSM rigorously, we also set the *feature proportion*

of our method as 1/16, resulting the comparable parameter number as them. Our method outperforms TSM by **1.89%** in terms of Top1 accuracy although TSM performs temporal modeling on more feature maps (1/8 of the input feature maps). Compared to GST, our method enhances the spatial features with the spatial-temporal information by *adding* instead of *replacing*. All of our baselines even including the RF-S model outperform GST, proving the superiority of retaining the complete spatial appearance prior learned on image tasks. GST has less parameters even than the simplest TSN because it sacrifices the channel number of spatial features, showing over-fitting when leveraging the ResNet101 as the backbone network.

The superiority of optimized feature fusion layer As shown in Tab. 2, when utilizing plain channel grouping operation between the spatial and the temporal filters, our method degenerates to the RF-L-Inception baseline and shows the most inferior performance for not synthesizing rich-scale spatial-temporal kernels. The synthesizing process relies on the irregular routing paths quantified by $ir - interactions$, which is 0 in this situation. The performance improves consistently with larger $ir - interactions$ and lower dropout rate. Notably, the dropout based fusion method (detailed in *supplementary material*) still outperforms the baseline largely while discarding a large proportion of spatial features, implying the synthesized *irregular-shaped* kernels measured by $ir - interactions$ have more direct impact on the final performance. Channel shuffling demonstrates the best performance under the premise of not introducing extra parameters. However, its performance

is worse than our method even without any regularization (45.01% vs. **45.44%**) because it is un-learnable and can not adjust the weights of the routing path dynamically for synthesizing the optimal kernels in a data-driven way. With the both two proposed regularizations ($\mathcal{L}_{interaction}$ and $\mathcal{L}_{capacity}$) activated, our method improves the performance by near another **1%**.

Studies on network details In the *supplementary material*, we show the ablation studies on *Where to insert the block?* and *What proportion of features need to be enhanced with space-temporal features?* Then, we demonstrate the studies on the detailed design of our block in Tab. 3, the pooling operation improves the performance significantly (**1.25%** Top1 accuracy) while our method is not sensitive to the specific implementation of the operation. The extra non-linearity introduced by the intermediate ReLU operations between spatial- and temporal- filters also benefits the performance obviously, which is consistent with the conclusion from previous work (Tran et al. 2018). The dilated convolution outperforms the ordinary convolution by **1.24%** in terms of Top5 accuracy even with less parameters, showing better generalization ability. Finally, we also try to decompose the spatial convolutions. As shown in the last block of Tab. 3, compared to the (2+1) D setting, the (1+1+1) D truly reduces negligible number of parameters but also degrades the performance.

Comparison with State-of-the-Art

Something-V1 The recognition performance obtained by our method is compared with state-of-the-art approaches that just use RGB frames, as shown in Tab. 4. The maximum RFS is $5 \times 5 \times 7$ by grid searching. The results *w.r.t.* the other RFSs is in the *supplementary material*. We also adopt this hyper-parameter for the other two datasets. The first block of the table shows the approaches that utilize Full-3D CNNs. The second block of the table lists methods leveraging 2D CNN or efficient 3D CNN implementation. From the table, it can be seen that our method results in an absolute gain of **+34.1%** (19.5% vs. 53.6%) over the TSN baseline. Our method performs better than 3D CNNs or heavier backbones with considerably less number of FLOPs. Under several common testing protocols, our method outperforms the most recent works significantly with comparable computational budget. Moreover, when adopting inputs of lower spatial resolution, *i.e.*, 112×112 , our method still achieves competitive result (**47.2%** top1 accuracy) with the recent methods such as TSM and GST, with much lower computation cost (**< 30%** of them). The analysis on the sensitivity of the methods to the input spatial resolution are in the *supplementary material* and demonstrates that our method show the lowest sensitivity.

Kinetics-400 As shown in Tab. 5, our method also captures rich object appearance cues effectively. Our method achieves inferior performance compared to some 3D CNN methods, *i.e.*, I3D and SlowFast networks. However, they both adopt much deeper and heavier 3D-ResNet-101 as the backbone network. They also leverage the inefficient non-local operation to model the long-range temporal dependen-

cies. When comparing with the methods based on 2D CNNs, our method outperforms them largely and demonstrates the best trade-off between the action recognition accuracy and the computation cost.

Diving48 To prove that our method can model long-term complex fine-grained motion cues and is not prone to over-fitting on few training samples, we test out method on Diving48. We input 16 frames to the network and sample only *one* or *two* clip from the video during inference. The results are shown in Tab. 6. Our method achieves significant improvement over the most recent state-of-the-arts, *i.e.*, over **1%** under the input of 16 frames.

Visualization

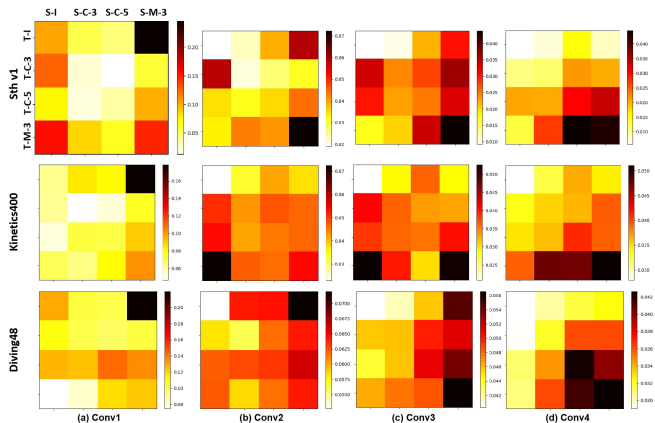


Figure 5: Visualization of spatial-temporal filter interactions of different layers (*i.e.*, Conv1 \sim 4) over multiple datasets. The deeper color, the denser interaction. The filters are denoted by a triplet-abbreviation, *i.e.*, “domain-type-kernelsize”, as shown in the vertical and horizontal axes of the up-left sub-figure. **S** and **T** denotes *spatial* and *temporal* domain, **C**, **M** and **I** denotes *convolution*, *max-pooling* and *identity*. For example, **S-C-3** denotes the spatial convolution with 3×3 kernel size. All the sub-figures share the same axes caption as the up-left one for brevity. *Best viewed by zooming in.*

To understand how spatial and temporal information are interacted in the *action perceptron synthesizer* to form the optimal kernel, we check the weights of the proposed *optimized feature fusion layer* in the synthesizer after each residual block of the ResNet-50 backbone, as shown in Fig. 5. Specifically, we quantize the importance of different shape interactions as the ℓ_1 norm of the corresponding transformation matrix, *i.e.*, \mathcal{T}_{ij} in Eq. (2). We first find that the over-all distribution learned on Something-Something v1 (first row) is non-sparse, indicating the rich-scale spatial-temporal modeling is necessary. Moreover, the max-pooling operation occupies considerable importance for serving as a hard attention strategy to find the local key contexts, which is consistent with the quantitative comparison in Tab. 3. Also, we find the receptive range of the operation evolves from spatial- to temporal- to spatial-temporal. We further visualize the statistics of the models trained on different datasets. For datasets requiring temporal information such

Method	Backbone	Pre-train	#Frames	GFLOPs	Top1 (%)	Top5 (%)
I3D (Carreira and Zisserman 2017)	3D-ResNet-50	Kinetics	32×3×2	153×3×2	41.6	72.2
GCN+Non-local (Wang and Gupta 2018)	3D-ResNet-50	Kinetics	32×3×2	303×3×2	46.1	76.8
ECO(En) (Zolfaghari, Singh, and Brox 2018)	BNInc + 3D-ResNet-18	Kinetics	92×1×1	267×1×1	46.4	-
TSN (Wang et al. 2016)	BN-Inception	ImageNet	8×1×1	16×1×1	19.5	-
MultiScale TRN (Zhou et al. 2018)	BN-Inception	ImageNet	8×1×1	16.37×1×1	34.4	63.2
R(2+1)D (Sudhakaran, Escalera, and Lanz 2020)	ResNet-34	Sports1M	32×1×1	152×1×1	45.7	-
S3D-G (Xie et al. 2018)	InceptionV1	ImageNet	64×1×1	71.38×1×1	48.2	78.7
STM (Jiang et al. 2019)	ResNet-50	ImageNet	16×3×10	67×3×10	50.7	80.4
TSM (Lin, Gan, and Han 2019)	ResNet-50	Kinetics	8×1×1	33×1×1	45.6	74.2
TSM (Lin, Gan, and Han 2019)	ResNet-50	Kinetics	16×1×1	65×1×1	47.2	77.1
GST (Luo and Yuille 2019)	ResNet-50	ImageNet	8×1×1	29.5×1×1	47.0	76.1
GST (Luo and Yuille 2019)	ResNet-50	ImageNet	16×1×1	59×1×1	48.6	77.9
TEA (Li et al. 2020)	ResNet-50	ImageNet	8×1×1	35×1×1	48.9	78.1
TEA (Li et al. 2020)	ResNet-50	ImageNet	16×1×1	70×1×1	51.9	80.3
TEA (Li et al. 2020)	ResNet-50	ImageNet	16×3×10	70×3×10	52.3	81.9
Ours	ResNet-50	ImageNet	8×1×1 [†]	9.12×1×1	47.2	75.6
	ResNet-50	ImageNet	8×1×1	36.19×1×1	50.8	80.6
	ResNet-50	ImageNet	16×1×1	72.38×1×1	53.6	83.1
	ResNet-50	ImageNet	16×3×10	36.19×3×10	54.1	84.3

Table 4: Comparison to state-of-the-art on Something-V1 validation set. [†] indicates the spatial resolution is of 112×112.

Method	Backbone	Pre-train	#Frames	GFLOPs	Top1 (%)	Top5 (%)
I3D (Carreira and Zisserman 2017)	Inception V1	ImageNet	64×N/A×N/A	108×N/A×N/A	72.1	90.3
I3D+NL (Wang et al. 2018b)	3D-ResNet-101	ImageNet	32×6×10	359×6×10	77.7	93.3
ECO(En) (Zolfaghari, Singh, and Brox 2018)	BNInc + 3D-ResNet-18	None	92×1×1	267×1×1	70.0	-
SlowFast (Feichtenhofer et al. 2019)	3D-ResNet-50	None	(4+32)×3×10	36.1×3×10	75.6	92.1
SlowFast+NL (Feichtenhofer et al. 2019)	3D-ResNet-101	None	(8+16)×3×10	234×3×10	79.8	93.9
TSN (Wang et al. 2016)	BN-Inception	ImageNet	25×10×1	53×10×1	69.1	88.7
R(2+1)D (Tran et al. 2018)	ResNet-34	None	32×1×10	152×1×10	72.0	90.0
TSM (Lin, Gan, and Han 2019)	ResNet-50	ImageNet	8×3×10	33×3×10	74.1	-
TSM (Lin, Gan, and Han 2019)	ResNet-50	ImageNet	16×3×10	65×3×10	74.7	-
STM (Jiang et al. 2019)	ResNet-50	ImageNet	16×3×10	67×3×10	73.7	91.6
TEA (Li et al. 2020)	ResNet-50	ImageNet	8×3×10	35×3×10	75.0	91.8
TEA (Li et al. 2020)	ResNet-50	ImageNet	16×3×10	70×3×10	76.1	92.5
Ours	ResNet-50	ImageNet	8×1×1	36.19×1×1	73.1	90.9
	ResNet-50	ImageNet	8×3×10	36.19×3×10	76.2	92.8
	ResNet-50	ImageNet	16×1×1	72.38×1×1	75.2	92.3
	ResNet-50	ImageNet	16×3×10	72.38×3×10	77.5	93.1

Table 5: Comparison to state-of-the-art on Kinetics-400.

Method	#Frames	Top1 (%)
TSN (from (Li, Li, and Vasconcelos 2018))	8	16.77
TRN (from (Li, Li, and Vasconcelos 2018))	8	22.8
P3D-ResNet50 (from (Luo and Yuille 2019))	16	32.4
C3D-ResNet50 (from (Luo and Yuille 2019))	16	34.5
(Kanojia, Kumawat, and Raman 2019)	64	35.64
GST (Luo and Yuille 2019)	16	38.8
CorrNet-101 (Wang et al. 2020)	32×10	38.6
GSM (Sudhakaran, Escalera, and Lanz 2020)	16×2	40.27
Ours	16	39.84
Ours	16×2	41.02

Table 6: Comparison to state-of-the-art on Diving48.

as Something-Something v1 (first row in Fig. 5) and Diving48 (third row in Fig. 5), we can see the models begin to aggregate the features by $3 \times 1 \times 1$ or $5 \times 1 \times 1$ temporal convolutions in the first stage, which is not learned out from Kinetics-400 in the early stage. Kinetics-400 involves richer spatial-temporal interactions in the second stage (as shown in the second column of the second row in Fig. 5) for its more diverse background scenes and more complicated ob-

ject interactions happening in the wild. Moreover, for stage 2, 3 and 4, compared to another two datasets, the most interactions of the model trained on Kinetics-400 concentrate on the temporal max-poolings instead of the temporal convolutions, which aligns with the fact that most action primitives in Kinetics are chronologically irrelevant.

We demonstrate more analysis *w.r.t.* the most improved classes by our method, action distribution in the feature space, action activation map and the temporal evolution of predictions in the *supplementary material*.

Conclusion

To tackle the essential spatial-temporal scale variances in videos, we propose to learn the optimal-scale kernels from the data and instantiate our method as the action percepton synthesizer block. We perform extensive evaluations to study its effectiveness on video action recognition task, achieving state-of-the-art results. We also demonstrate some visualization results for more intuitive understanding of our method.

References

- Carreira, J.; and Zisserman, A. 2017. Quo vadis, action recognition? a new model and the kinetics dataset. In *proceedings of the IEEE Conference on Computer Vision and Pattern Recognition*, 6299–6308.
- Dai, J.; Qi, H.; Xiong, Y.; Li, Y.; Zhang, G.; Hu, H.; and Wei, Y. 2017. Deformable convolutional networks. In *Proceedings of the IEEE international conference on computer vision*, 764–773.
- Deng, J.; Dong, W.; Socher, R.; Li, L.-J.; Li, K.; and Fei-Fei, L. 2009. Imagenet: A large-scale hierarchical image database. In *2009 IEEE conference on computer vision and pattern recognition*, 248–255. Ieee.
- Feichtenhofer, C.; Fan, H.; Malik, J.; and He, K. 2019. Slow-fast networks for video recognition. In *Proceedings of the IEEE international conference on computer vision*, 6202–6211.
- Feichtenhofer, C.; Pinz, A.; and Zisserman, A. 2016. Convolutional two-stream network fusion for video action recognition. In *Proceedings of the IEEE conference on computer vision and pattern recognition*, 1933–1941.
- Goyal, R.; Kahou, S. E.; Michalski, V.; Materzynska, J.; Westphal, S.; Kim, H.; Haenel, V.; Fruend, I.; Yianilos, P.; Mueller-Freitag, M.; et al. 2017. The ” Something Something” Video Database for Learning and Evaluating Visual Common Sense. In *ICCV*, volume 1, 5.
- Hara, K.; Kataoka, H.; and Satoh, Y. 2017. Learning spatio-temporal features with 3D residual networks for action recognition. In *Proceedings of the IEEE International Conference on Computer Vision Workshops*, 3154–3160.
- He, K.; Zhang, X.; Ren, S.; and Sun, J. 2016. Deep residual learning for image recognition. In *Proceedings of the IEEE conference on computer vision and pattern recognition*, 770–778.
- Hinton, G. E.; Srivastava, N.; Krizhevsky, A.; Sutskever, I.; and Salakhutdinov, R. R. 2012. Improving neural networks by preventing co-adaptation of feature detectors. *arXiv preprint arXiv:1207.0580* .
- Ioffe, S.; and Szegedy, C. 2015. Batch normalization: Accelerating deep network training by reducing internal covariate shift. *arXiv preprint arXiv:1502.03167* .
- Jiang, B.; Wang, M.; Gan, W.; Wu, W.; and Yan, J. 2019. Stm: Spatiotemporal and motion encoding for action recognition. In *Proceedings of the IEEE International Conference on Computer Vision*, 2000–2009.
- Kanojia, G.; Kumawat, S.; and Raman, S. 2019. Attentive spatio-temporal representation learning for diving classification. In *Proceedings of the IEEE Conference on Computer Vision and Pattern Recognition Workshops*, 0–0.
- Krizhevsky, A.; Sutskever, I.; and Hinton, G. E. 2012. Imagenet classification with deep convolutional neural networks. In *Advances in neural information processing systems*, 1097–1105.
- Li, Y.; Ji, B.; Shi, X.; Zhang, J.; Kang, B.; and Wang, L. 2020. TEA: Temporal Excitation and Aggregation for Action Recognition. In *Proceedings of the IEEE/CVF Conference on Computer Vision and Pattern Recognition*, 909–918.
- Li, Y.; Li, Y.; and Vasconcelos, N. 2018. Resound: Towards action recognition without representation bias. In *Proceedings of the European Conference on Computer Vision (ECCV)*, 513–528.
- Lin, J.; Gan, C.; and Han, S. 2019. Tsm: Temporal shift module for efficient video understanding. In *Proceedings of the IEEE International Conference on Computer Vision*, 7083–7093.
- Luo, C.; and Yuille, A. L. 2019. Grouped spatial-temporal aggregation for efficient action recognition. In *Proceedings of the IEEE International Conference on Computer Vision*, 5512–5521.
- Ma, N.; Zhang, X.; Zheng, H.-T.; and Sun, J. 2018. Shufflenet v2: Practical guidelines for efficient cnn architecture design. In *Proceedings of the European conference on computer vision (ECCV)*, 116–131.
- Mahdisoltani, F.; Berger, G.; Gharbieh, W.; Fleet, D.; and Memisevic, R. 2018. Fine-grained video classification and captioning. *arXiv preprint arXiv:1804.09235* 5(6).
- Nair, V.; and Hinton, G. E. 2010. Rectified linear units improve restricted boltzmann machines. In *ICML*.
- Paszke, A.; Gross, S.; Massa, F.; Lerer, A.; Bradbury, J.; Chanan, G.; Killeen, T.; Lin, Z.; Gimelshein, N.; Antiga, L.; et al. 2019. Pytorch: An imperative style, high-performance deep learning library. In *Advances in neural information processing systems*, 8026–8037.
- Piergiovanni, A.; Angelova, A.; and Ryoo, M. S. 2019. Tiny Video Networks. *arXiv preprint arXiv:1910.06961* .
- Qiu, Z.; Yao, T.; and Mei, T. 2017. Learning spatio-temporal representation with pseudo-3d residual networks. In *proceedings of the IEEE International Conference on Computer Vision*, 5533–5541.
- Sandler, M.; Howard, A.; Zhu, M.; Zhmoginov, A.; and Chen, L.-C. 2018. Mobilenetv2: Inverted residuals and linear bottlenecks. In *Proceedings of the IEEE conference on computer vision and pattern recognition*, 4510–4520.
- Simonyan, K.; and Zisserman, A. 2014a. Two-stream convolutional networks for action recognition in videos. In *Advances in neural information processing systems*, 568–576.
- Simonyan, K.; and Zisserman, A. 2014b. Very deep convolutional networks for large-scale image recognition. *arXiv preprint arXiv:1409.1556* .
- Sudhakaran, S.; Escalera, S.; and Lanz, O. 2020. Gate-Shift Networks for Video Action Recognition. In *Proceedings of the IEEE/CVF Conference on Computer Vision and Pattern Recognition*, 1102–1111.
- Szegedy, C.; Ioffe, S.; Vanhoucke, V.; and Alemi, A. A. 2017. Inception-v4, inception-resnet and the impact of residual connections on learning. In *Thirty-first AAAI conference on artificial intelligence*.

- Szegedy, C.; Liu, W.; Jia, Y.; Sermanet, P.; Reed, S.; Anguelov, D.; Erhan, D.; Vanhoucke, V.; and Rabinovich, A. 2015. Going deeper with convolutions. In *Proceedings of the IEEE conference on computer vision and pattern recognition*, 1–9.
- Szegedy, C.; Vanhoucke, V.; Ioffe, S.; Shlens, J.; and Wojna, Z. 2016. Rethinking the inception architecture for computer vision. In *Proceedings of the IEEE conference on computer vision and pattern recognition*, 2818–2826.
- Tian, Y.; Che, Z.; Bao, W.; Zhai, G.; and Gao, Z. 2020. Self-supervised Motion Representation via Scattering Local Motion Cues .
- Tian, Y.; Min, X.; Zhai, G.; and Gao, Z. 2019. Video-based early asd detection via temporal pyramid networks. In *2019 IEEE International Conference on Multimedia and Expo (ICME)*, 272–277. IEEE.
- Tran, D.; Bourdev, L.; Fergus, R.; Torresani, L.; and Paluri, M. 2015. Learning spatiotemporal features with 3d convolutional networks. In *Proceedings of the IEEE international conference on computer vision*, 4489–4497.
- Tran, D.; Wang, H.; Torresani, L.; Ray, J.; LeCun, Y.; and Paluri, M. 2018. A closer look at spatiotemporal convolutions for action recognition. In *Proceedings of the IEEE conference on Computer Vision and Pattern Recognition*, 6450–6459.
- Wang, H.; Tran, D.; Torresani, L.; and Feiszli, M. 2020. Video Modeling with Correlation Networks. In *Proceedings of the IEEE/CVF Conference on Computer Vision and Pattern Recognition*, 352–361.
- Wang, L.; Xiong, Y.; Wang, Z.; Qiao, Y.; Lin, D.; Tang, X.; and Van Gool, L. 2016. Temporal segment networks: Towards good practices for deep action recognition. In *European conference on computer vision*, 20–36. Springer.
- Wang, L.; Xiong, Y.; Wang, Z.; Qiao, Y.; Lin, D.; Tang, X.; and Van Gool, L. 2018a. Temporal segment networks for action recognition in videos. *IEEE transactions on pattern analysis and machine intelligence* 41(11): 2740–2755.
- Wang, X.; Girshick, R.; Gupta, A.; and He, K. 2018b. Non-local neural networks. In *Proceedings of the IEEE conference on computer vision and pattern recognition*, 7794–7803.
- Wang, X.; and Gupta, A. 2018. Videos as space-time region graphs. In *Proceedings of the European conference on computer vision (ECCV)*, 399–417.
- Xie, S.; Girshick, R.; Dollár, P.; Tu, Z.; and He, K. 2017. Aggregated residual transformations for deep neural networks. In *Proceedings of the IEEE conference on computer vision and pattern recognition*, 1492–1500.
- Xie, S.; Sun, C.; Huang, J.; Tu, Z.; and Murphy, K. 2018. Rethinking spatiotemporal feature learning: Speed-accuracy trade-offs in video classification. In *Proceedings of the European Conference on Computer Vision (ECCV)*, 305–321.
- Zhang, X.; Zhou, X.; Lin, M.; and Sun, J. 2018. Shufflenet: An extremely efficient convolutional neural network for mobile devices. In *Proceedings of the IEEE conference on computer vision and pattern recognition*, 6848–6856.
- Zhou, B.; Andonian, A.; Oliva, A.; and Torralba, A. 2018. Temporal relational reasoning in videos. In *Proceedings of the European Conference on Computer Vision (ECCV)*, 803–818.
- Zolfaghari, M.; Singh, K.; and Brox, T. 2018. Eco: Efficient convolutional network for online video understanding. In *Proceedings of the European conference on computer vision (ECCV)*, 695–712.
- Zoph, B.; and Le, Q. V. 2016. Neural architecture search with reinforcement learning. *arXiv preprint arXiv:1611.01578* .